

Strain-Modulated Exchange-Spring Magnetic Behavior in Amorphous Tb-Fe Thin Films

Taehwan Lee,¹ Mohanchandra Kotekar Panduranga,² Chang Wan Han,³
Volkan Ortalan,³ and Gregory Paul Carman^{1,2,*}

¹*Department of Materials Science and Engineering, University of California,
Los Angeles, California 90095, USA*

²*Department of Mechanical and Aerospace Engineering, University of California,
Los Angeles, California 90095, USA*

³*School of Materials Engineering, Purdue University, West Lafayette, Indiana 47907, USA*

(Received 17 January 2017; revised manuscript received 24 May 2017; published 25 August 2017)

This paper studies the room-temperature exchange-spring magnetic behavior of amorphous TbFe films subjected to an applied strain. The cross-sectional composition measurement of the sputter-deposited TbFe film shows a compositional gradient through the thickness. The gradient is near the compensation composition of amorphous TbFe film producing a Tb-dominant region and a Fe-dominant region. The as-deposited film shows a two-step switching behavior with a negative coercive field, while an applied compressive (or tensile) strain eliminates (or enhances) the two-step switching behavior. The strain influence is attributed to the TbFe composition gradient and relatively large magnetoelastic property of the Tb-dominant region as compared to the Fe-dominant one.

DOI: 10.1103/PhysRevApplied.8.024024

I. INTRODUCTION

Voltage-induced strain modulation of magnetic materials is receiving considerable attention due to its potential for producing extremely energy-efficient spintronic memory devices [1–4]. While several research studies have been conducted on various material systems such as Ni/PMN-PT (or PZT), Co-Fe-B/PMN-PT (or PZT), and Fe-Ga-B/PZT [2,5–8], the voltage-induced strain approach typically rotates the magnetization by only 90° rather than 180° desired in magnetic memory bits. To overcome this restriction, different geometries and operating approaches have been investigated [7,9–11], but these result in larger bit layouts or dynamic timing that poses problems. Here, we experimentally demonstrate a magnetic reversal approach using exchange-spring magnetic (ESM) behavior that promises a 180° switching using voltage-induced mechanical strain.

Exchange-spring magnets containing negatively coupled soft and hard magnetic phases have been extensively studied due to their abnormal magnetic behavior and high potential in spintronic applications. Most ESM systems have a major shortcoming that limits them to an immovable magnetic response (e.g., coercivity and remanence). Therefore, new ESM studies focusing on controlling *in situ* magnetic properties are needed. In this work, a compositionally graded amorphous TbFe film near the compensation composition shows the room-temperature ESM response modulated with an applied mechanical strain.

Several ESM studies have evaluated a variety of materials displaying distinct switching steps and negative coercivity values. For example, experimental evaluation of DyFe₂/YFe₂ superlattices [12–18], Fe/Sm-Co [19],

Ni₈₀Fe₂₀/Sm-Co(Sm-Fe) [20,21], or Gd-Fe/Tb-Fe [22,23] bilayers have been used to understand and explain the physical origins of exchange-spring magnets but all at low temperature. In these studies, the ESM properties are modified by changing the layer's thickness ratio or selecting a material with a different magnetocrystalline anisotropy. This selection produces ESM materials whose magnetic response is fixed and cannot be modified once fabricated. On the other hand, several studies have evaluated Tb-Fe(Co) thin films and bulk Tb-Fe material properties near the compensation composition [24–29]. These studies show the magnetostriction coefficients (λ_s) are strongly dependent on the composition, with Tb-dominant compositions producing much higher λ_s than Fe-dominant compositions [24]. This λ_s difference provides an opportunity to control an ESM material using the induced magnetoelastic anisotropy.

In this paper, we demonstrate a room-temperature ESM behavior in a compositionally graded TbFe thin film near the compensation composition. The Tb-dominant and Fe-dominant phases formed by the composition gradient in TbFe film act as hard and soft magnetic layers in ESM structure. The *M-H* behavior of this ESM structure is explained using the major and minor spins present in the respective phases and their coupling states. When subjected to a mechanical load, the film's separated switching steps and negative coercive behavior are modulated and eliminated due to the higher magnetostriction present in the Tb-dominant layer.

II. EXPERIMENTAL DETAILS

Amorphous TbFe films are deposited on 4-in-diameter Si(100) substrates using a dc-sputtering technique.

*carman@seas.ucla.edu

A TbFe₂ alloy target is mounted in the sputtering systems, and the sputtering parameters of base pressure below 2×10^{-6} Torr, 3×10^{-3} Torr Ar gas pressure, 248-W sputtering power, and a rotating substrate stage are used for the deposition. Cross-sectional transmission-electron-microscopy samples are prepared by the *in situ* lift-out method using an FEI Nova 600 DualBeam microscope. Compositional analysis is conducted using an Oxford X-Max 80T EDS (energy-dispersive x-ray spectroscopy) equipped within an FEI Titan 80-300 scanning-transmission-electron microscope (STEM). EDS line profiles are obtained with annular-dark-field STEM mode, and the relative atomic composition profiles along the film thickness is determined by the Cliff-Lorimer method [30], which is implemented in Oxford AZTEC software. The film's amorphous state is confirmed with a Bruker D8 DISCOVER x-ray diffractometer showing the absence of any peaks in a range of 2θ from 15° to 60° .

SQUID (superconducting-quantum-interference device) and MOKE (magneto-optic Kerr effect) systems are used to measure the magnetic hysteresis curves of the film. Room-temperature SQUID measurements provide magnetization and coercive field values under 2-T fields. MOKE magnetic hysteresis loops in the longitudinal mode are measured in the presence of mechanical strain. For this test, a 2.5×0.5 cm² sample is diced from the TbFe film on a 4-in Si wafer and placed in a four-point bending jig capable of applying tensile or compressive strains depending upon the film orientation (see the insets of Fig. 3) [31]. Strain gauges attached to the backside of the sample measure the applied strain.

III. RESULTS AND DISCUSSION

Figure 1 shows the variation of Tb and Fe atomic percent as a function of film thickness. The 0.09- μ m location represents the TbFe/Si substrate interface, while the 0.38 μ m represents the Pt/TbFe interface. The spurious

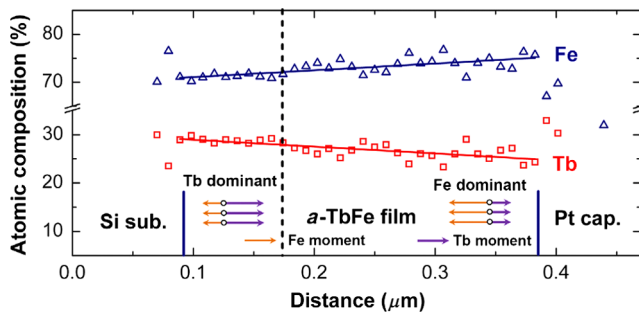


FIG. 1. Atomic composition variation of Tb and Fe as a function of film thickness. Amorphous TbFe film ranges from 0.09 μ m (bottom) to 0.38 μ m (top). A dashed vertical line marks the compensation composition of TbFe film, and arrow schematics represent the Tb- and Fe-dominated regions based on the compensation composition.

data at distances <0.09 or >0.38 μ m are quantification errors due to the negligible Tb and Fe x-ray counts from the Si substrate or Pt capping. For the TbFe alloy film, the Tb atomic percent decreases from 29.1 at. % (bottom) to 24.9 at. % (top), while the Fe increases from 70.9 at. % (bottom) to 75.1 at. % (top) in a fairly linear fashion. The composition variation is caused by target heating during deposition producing different sputtering yields for each atomic component [32].

Figure 2 shows SQUID data for magnetization M versus magnetic field H measured along the in-plane direction of the film. Figure 2(a) represents truncated hysteresis cycles (± 1200 Oe) for measurements between ± 2 T with arrows representing decreasing H values or the “sweep-down” curve. The magnetization at 2 T, while not shown, is 108 emu/cc. The smaller magnetization value 50 emu/cc at 1200 Oe is attributed to the relatively large high-field susceptibility of amorphous TbFe [33]. Figure 2(a) clearly shows two-step switching for decreasing H values

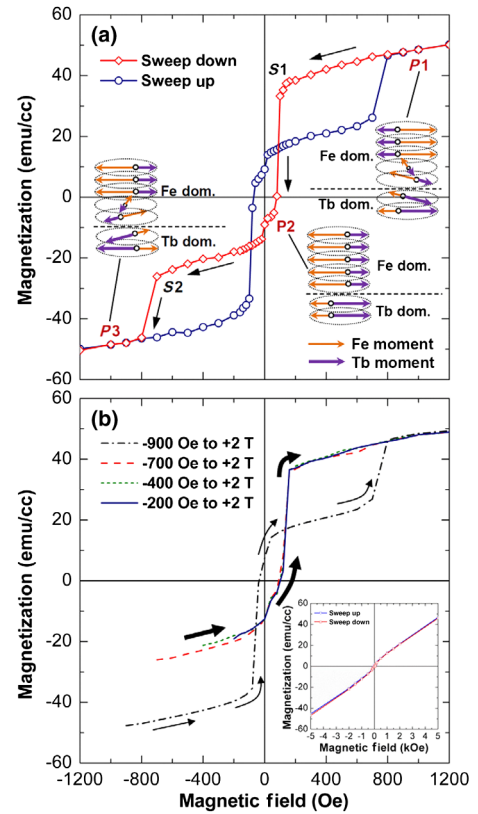


FIG. 2. M - H curves for TbFe film. (a) H field is swept between ± 2 T but truncated to show ± 1200 Oe. Two switching steps (S1 and S2) are marked on a sweep-down curve. Arrow schematics show the Tb and Fe spin configuration at the corresponding points (P1–P3) in a sweep-down curve. (b) Sweep-up curves from four different H fields (-200 , -400 , -700 , and -900 Oe) of minor loops. Sweep-down curves, which are identical to the one in (a), are not shown. Thicker and thinner arrows are marked to show different trajectories. (Inset) M - H loop of the TbFe film with a magnetic field applied normal to the film plane.

(sweep-down) as well as increasing values (sweep-up). During sweep-down, the first switching (marked as $S1$) occurs at $+90$ Oe producing a negative coercivity of -80 Oe and negative remanence of -9 emu/cc. The second switching (marked as $S2$) occurs at -750 Oe. When the sweeping direction is reversed from negative saturation (i.e., -2 T), similar two steps are observed including negative coercive field and negative remanence values.

The physics producing the two-step switching and negative coercive behavior are discussed with the use of Fig. 1. TbFe is a rare-earth–transition-metal (R - M) ferrimagnetic material with two antiparallel aligned Tb and Fe spins. The alloy's composition, as well as the operating temperature, dictates the effective magnetic moment. The compensation composition represented by the alloy's net magnetic moment vanishing is depicted by a dashed vertical line (28 Tb at. %) in Fig. 1[24]. The corresponding magnetic property variation across this vertical line is relatively sharp creating two separate regions with either Tb-dominant or Fe-dominant magnetic moments. This gradient-induced separation is contrasted with conventional systems where the magnetic properties change across an atomically sharp interface [12–18]. The illustrations in Fig. 1 show two regions magnetically dominated by either the Tb or Fe spins. The Tb atomic magnetic moment is represented with a darker arrow compared to the Fe moment, and the arrow's length identifies the Fe-dominated region (adjacent to Pt) or the Tb-dominated region (adjacent to Si). These two regions produce the magnetic response observed in Fig. 2(a).

The two-step switching and negative coercive field shown in Fig. 2(a) is caused by the presence of both the Fe- and Tb-dominated regions as well as the exchange coupling between them. The interface exchange coupling for three points ($P1$ - $P3$) along the sweep-down portion of the M - H curve is illustrated with arrows in the schematics of Fig. 2(a). The exchange coupling at the interface derives from ferromagnetic Fe-Fe spin interaction between the Fe- and Tb-dominant regions [34]. When a magnetic field is applied to the material, the exchange coupling between the Tb-dominant region and the Fe-dominant region has competition with the applied magnetic field energy. Specifically, The Tb spin in the Tb-dominant region, as well as the Fe in the Fe-dominant region, tend to align with the magnetic field which is in direct competition with the Fe-Fe spin interaction between the two regions. All the schematic spin arrows [Fig. 2(a)] represent in-plane orientations with any deviations from the horizontal, signifying in-plane canting angles of interface spins. At $P1$ in Fig. 2(a), the spins farthest from the interface (i.e., either Tb or Fe dominant) wind to align towards the magnetic field direction. However, the interface spins in the Tb- and Fe-dominant layers cant (i.e., in plane of the film) to accommodate the competition between the magnetic field

aligning the net magnetic moment and the ferromagnetic Fe-Fe spin interaction. This competition creates a transition region between the canted spins and wound spins. The transition region thickness in the Fe-dominant region is larger than the Tb-dominant one due to the magnetically softer Fe-dominant region properties as compared to the Tb-dominant region. As the magnetic field is decreased from $P1$ toward $P2$, the Fe-dominant transition region grows, and at 90 Oe ($S1$), all the Fe spins (see $P2$ illustration) in the Fe-dominated region flip. This point represents where the exchange-coupling energy dominates the applied H -field energy resulting in a complete reversal of the Fe spins in the Fe-dominated region. At $H = 0$, the flipped Fe spins produce a negative remanence value. As the field approaches $P3$, the Tb-dominant region flips in the presence of a sufficiently large negative field which overcomes the intrinsic magnetic anisotropy of the Tb-dominated region. At $P3$, the magnetic moments are 180° out of phase with spin orientations illustrated by $P1$. This process represents an exchange-spring magnet with anti-ferromagnetic exchange coupling as described in previous ferrimagnetic multilayers [12–18].

Generally, there are other mechanisms that can produce a negative coercive field such as an exchange bias and/or dual magnetic anisotropy. However, these possibilities are ruled out with experimental tests conducted on the sample. First, in some cases, high magnetic fields can cause the exchange-bias field to change directions [35]. This directional change may result in an apparent negative coercive field in a symmetric manner. Figure 2(b) shows minor sweep-up M - H curves for the same film presented in Fig. 2(a). The minor curves are measured by first saturating the film to $+2$ T and then reducing the field (i.e., sweep-down) to one of four values (i.e., -200 , -400 , -700 , and -900 Oe), while not shown in the figure. The M - H curves in Fig. 2(b) show data for the increasing H field from one of these four values, i.e., sweep-up curves. As can be seen, three of these minor loops (i.e., -200 , -400 , and -700 Oe thicker arrows) overlap and follow the path of the sweep-down curve presented in Fig. 2(a). These overlaps arise due to the reversible rotation of Fe moments in the Fe-dominant region after passing through $S1$. On the other hand, the Fig. 2(b) sweep-up curve from -900 Oe shows an entirely different trajectory (marked with thinner arrows) from the other curves. This difference is produced by the irreversible flip of the hard magnetic Tb-dominant region at $S2$. The reversible minor loop behavior for -200 , -400 , and -700 Oe while absent for -900 Oe (i.e., before reaching a hard magnetic phase switching) ensures that the first switching reflects the unwinding of the spins in the Fe-dominant region by exchange coupling [36]. This reversible behavior at relatively small applied magnetic fields rules out the possibility that the observed negative coercive response is an exchange-bias mechanism.

One must also consider the possibility that two different anisotropies may be present to produce an apparent negative coercive field [37]. This is a concern because some studies report a perpendicular magnetic anisotropy in amorphous TbFe films which is attributed to deposition parameters [38,39]. To eliminate the dual magnetic anisotropy from consideration, M - H loops in different in-plane directions as well as the out-of-plane direction are measured. All in-plane M - H measurements show similar results presented in Fig. 2(a) revealing that the film is magnetically isotropic in plane. The M - H loop measured out of plane presented in the inset of Fig. 2(b) shows a linear hard axis curve without hysteresis, clearly indicating the magnetic moments are all in plane. Therefore, the dual magnetic anisotropy explanation is ruled out for the negative coercive field. This experimental verification leads us to conclude with reasonable certainty that the origin of negative coercive field is the exchange coupling between Fe- and Tb-dominant regions which can be controlled with an applied mechanical strain.

Figure 3 presents MOKE M - H loops (i.e., in-plane measurements) measured at three different mechanical strains, i.e., 0, -820 , and $+540$ $\mu\epsilon$ (microstrain). Since the TbFe 290-nm film is much thinner than 500- μm Si substrate, the film's strain is essentially uniform through the thickness. All strain values are discussed in terms of the film's strain rather than the Si substrate's strain. Figure 3(a)

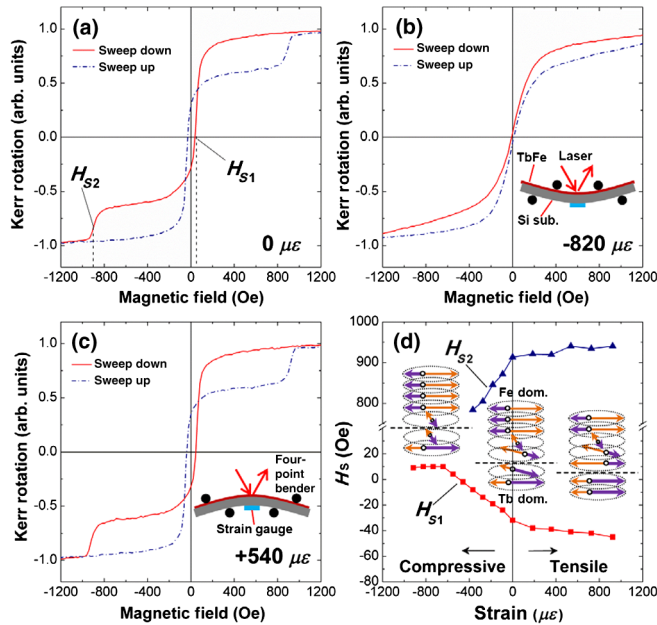


FIG. 3. MOKE M - H curves measured at three different mechanical strains, 0, -820 , and $+540$ $\mu\epsilon$ (a)–(c). Insets in (b) and (c) indicate the four-point bending fixture used to apply mechanical strain. The first and second switching-field [see H_{S1} and H_{S2} marked in (a)] variations as a function of mechanical strain (d). The arrow illustrations show the change of the exchange-coupling state depending on mechanical strain.

measured at 0 $\mu\epsilon$ resembles the SQUID results shown in Fig. 2(a) including the two-step and negative coercive behavior. The small differences in switching field values are caused by the MOKE measurement's limited sampling area as well as penetration depth. The Fig. 3(b) M - H loop measured at -820 $\mu\epsilon$ (i.e., compressive strain) eliminates the two-step switching and the negative coercive field. Figure 3(c) measured at $+540$ $\mu\epsilon$ (i.e., tensile strain), slightly enhances the two-step switching with absolute magnitudes of switching fields increasing by 28% (for $S1$) and 3% (for $S2$) compared to Fig. 3(a).

Figure 3(d) plots the first and second switching fields [see H_{S1} and H_{S2} in Fig. 3(a)] as a function of mechanical strain. As the applied compressive strain increases from zero, the H_{S1} value becomes less negative and switches to positive (-32 to $+10$ Oe) values. On the other hand, H_{S2} becomes less positive, i.e., linearly decreases from 913 to 784 Oe. For increasing tensile strain values, H_{S1} becomes more negative (-32 to -45 Oe), while H_{S2} becomes more positive (913 to 941 Oe). The functional dependence of H_{S1} and H_{S2} on strain is attributed to the induced magnetoelastic anisotropy. The strain-induced magnetic anisotropy is defined to be $K = \frac{3}{2}\lambda_s E \epsilon$, where E is Young's modulus, λ_s is the magnetostriction coefficient, and ϵ is the strain applied. The λ_s values are a function of the relative Tb/Fe composition [24] with the Tb-dominant (Tb $>$ 28 at. %) shown in Fig. 1) region 2 orders of magnitude larger than the Fe-dominant (Tb $<$ 28 at. %) region. Therefore, the applied strains significantly change the magnetic anisotropy of the Tb-dominant region, while the Fe-dominant region remains relatively unchanged. Thus, an applied strain increases (or decreases) H_{S2} under tensile (compressive) strain. The three schematics on the left, middle, and right sides in Fig. 3(d) illustrate the magnetic spin states at $P1$ of Fig. 2(a) under applied compressive, zero, and tensile strains, respectively. All arrows in these drawings represent in-plane orientations with off-horizontal interface spin arrows representing in-plane canting. As a tensile strain is applied to this system (schematic right), the Tb-dominant canting region is essentially eliminated, while the Fe-dominant region size substantially increases compared to without a strain (schematic middle). This feature is caused by the large magnetostriction present in the Tb-dominant region. In general, the smaller the canting angle of the Tb-dominant phase, the broader the transition region in the Fe-dominant region. For compressive strains, the canting angle in the Tb-dominant region increases, while the size of the transition in the Fe-dominant region decreases, i.e., exactly converse to an applied positive strain. These applied strains produce larger negative H_{S1} values under a tensile strain, while smaller negative or even positive H_{S1} under a compressive strain.

This sign change of coercive field and remanent magnetization represents a potential for the magnetic reversal up to 180° using the applied strain. This strain-applied

ESM switching mechanism can be used in future memory devices if more studies are conducted to overcome some practical problems such as stability of a switched state. For these later devices, a voltage-induced strain would be implemented as suggested by other researchers [3–10].

IV. CONCLUSION

In conclusion, exchange-spring magnetic behavior has been experimentally observed in a compositionally graded amorphous TbFe thin film at room temperature. The gradient through the TbFe film thickness produces Tb- and Fe-dominant regions, and their exchange coupling at the interface creates an exchange-spring magnetic behavior. By applying a mechanical strain to the film, a two-step switching with the negative coercive field is both modulated and eliminated showing the promise of 180° switching. The modulation is caused by the relatively higher magnetostriction coefficient in the Tb-dominant region compared to the Fe-dominant region, producing larger changes in magnetic anisotropy as the strain is applied. This reversal character, via exchange coupling, is directly applicable to a range of spintronic devices including memory elements due to its directional switching with extremely low energy consumption.

ACKNOWLEDGMENTS

This work is supported in part by FAME, one of six centers of STARnet, a Semiconductor Research Corporation program sponsored by MARCO and DARPA, and NSF Nanosystems Engineering Research Center for Translational Applications of Nanoscale Multiferroic Systems (TANMS) Cooperative Agreement Award No. EEC-1160504.

-
- [1] Y. T. Yang, J. Li, X. L. Peng, X. Q. Wang, D. H. Wang, Q. Q. Cao, and Y. W. Du, Electric-field mediated non-volatile tuning magnetism in CoPt/PMN-PT heterostructure for magnetoelectric memory devices, *J. Appl. Phys.* **119**, 073909 (2016).
- [2] Ren-Ci Peng, Jia-Mian Hu, Kasma Momeni, Jian-Jun Wang, Long-Qing Chen, and Ce-Wen Nan, Fast 180° magnetization switching in a strain-mediated multiferroic heterostructure driven by a voltage, *Sci. Rep.* **6**, 27561 (2016).
- [3] Jia-Mian Hu, Zheng Li, Jing Wang, and C. W. Nan, Electric-field control of strain-mediated magnetoelectric random access memory, *J. Appl. Phys.* **107**, 093912 (2010).
- [4] Jia-Mian Hu, Zheng Li, Long-Qing Chen, and Ce-Wen Nan, High-density magnetoresistive random access memory operating at ultralow voltage at room temperature, *Nat. Commun.* **2**, 553 (2011).
- [5] Alexander Tkach, Andreas Kehlberger, Felix Buttner, Gerhard Jakob, Stefan Eisebitt, and Mathias Klau, Electric field modification of magnetotransport in Ni thin films on (011) PMN-PT piezoelectrodes, *Appl. Phys. Lett.* **106**, 062404 (2015).
- [6] Tao Wu, Alexandre Bur, Kin Wong, Ping Zhao, Christopher S. Lynch, Pedram Khalili Amiri, Kang L. Wang, and Gregory P. Carman, Electrical control of reversible, and permanent magnetization reorientation for magnetoelectric memory devices, *Appl. Phys. Lett.* **98**, 262504 (2011).
- [7] T. X. Nan, Z. Y. Zhou, J. Lou, M. Liu, X. Yang, Y. Gao, S. Rand, and N. X. Sun, Voltage impulse induced bistable magnetization switching in multiferroic heterostructures, *Appl. Phys. Lett.* **100**, 132409 (2012).
- [8] Hyungsuk K. D. Kim, Laura T. Schelhas, Scott Keller, Joshua L. Hockel, Sarah H. Tolbert, and Gregory P. Carman, Magnetoelectric control of superparamagnetism, *Nano Lett.* **13**, 884 (2013).
- [9] Yajie Chen, Trifon Fitchorov, Carmine Vittoria, and V. G. Harris, Electrically controlled magnetization switching in a multiferroic heterostructure, *Appl. Phys. Lett.* **97**, 052502 (2010).
- [10] Jizhai Cui, Joshua L. Hockel, Paul K. Nordeen, David M. Pisani, Cheng-yen Liang, Gregory P. Carman, and Christopher S. Lynch, A method to control magnetism in individual strain-mediated magnetoelectric islands, *Appl. Phys. Lett.* **103**, 232905 (2013).
- [11] Xu Li, Dorinamaria Carka, Cheng-yen Liang, Abdou E. Sepulveda, Scott M. Keller, Pedram Khalili Amiri, Gregory P. Carman, and Christopher S. Lynch, Strain-mediated 180° perpendicular magnetization switching of a single domain multiferroic structure, *J. Appl. Phys.* **118**, 014101 (2015).
- [12] K. Dumesnil, M. Dutheil, C. Dufour, and Ph. Mangin, Spring magnet behavior in DyFe₂/YFe₂ Laves phases superlattices, *Phys. Rev. B* **62**, 1136 (2000).
- [13] M. Sawicki, G. J. Bowden, P. A. J. de Groot, B. D. Rainford, J.-M. L. Beaujour, R. C. C. Ward, and M. R. Wells, Exchange springs in antiferromagnetically coupled DyFe₂-YFe₂ superlattices, *Phys. Rev. B* **62**, 5817 (2000).
- [14] M. Sawicki, G. J. Bowden, P. A. J. de Groot, B. D. Rainford, R. C. C. Ward, and M. R. Wells, Magnetic properties of epitaxial (110) multilayer films of DyFe₂ and YFe₂, *J. Appl. Phys.* **87**, 6839 (2000).
- [15] K. Dumesnil, C. Dufour, Ph. Mangin, A. Rogalev, and F. Wilhelm, Temperature dependence in the magnetization reversal process of DyFe₂/YFe₂ exchange-coupled superlattices, *J. Phys. Condens. Matter* **17**, L215 (2005).
- [16] G. B. G. Stenning *et al.*, Magnetic reversal in a YFe₂ dominated DyFe₂/YFe₂ multilayer film, *Appl. Phys. Lett.* **101**, 072412 (2012).
- [17] G. B. G. Stenning, G. J. Bowden, S. A. Gregory, P. A. J. de Groot, G. van der Laan, L. R. Shelford, P. Bencok, P. Steadman, A. N. Dobrynin, and T. Hesjedal, Transverse magnetic exchange springs in a DyFe₂/YFe₂ superlattice, *Phys. Rev. B* **86**, 174420 (2012).
- [18] G. B. G. Stenning, G. J. Bowden, P. A. J. de Groot, G. van der Laan, A. I. Figueroa, P. Bencok, P. Steadman, and T. Hesjedal, Magnetic reversal in Dy-doped DyFe₂/YFe₂ superlattice film, *Phys. Rev. B* **91**, 094403 (2015).
- [19] J. E. Davies, O. Hellwig, Eric. E. Fullerton, J. S. Jiang, S. D. Bader, G. T. Zimányi, and K. Liu, Anisotropy dependence of irreversible switching in Fe/SmCo and FeNi/FePt

- exchange spring magnet film, *Appl. Phys. Lett.* **86**, 262503 (2005).
- [20] J. Y. Gu, J. Burgess, and Chun-Yeol You, Temperature dependence of magnetization reversal processes in exchange-spring magnets, *J. Appl. Phys.* **107**, 103918 (2010).
- [21] J. Y. Gu, J. Kusnadi, and Chun-Yeol You, Proximity effect in a superconductor/exchange-spring-magnet hybrid system, *Phys. Rev. B* **81**, 214435 (2010).
- [22] S. Mangin, T. Hauet, Y. Henry, F. Montaigne, and Eric E. Fullerton, Influence of lateral domains and interface domain walls on exchange-bias phenomena in GbFe/TdFe bilayers, *Phys. Rev. B* **74**, 024414 (2006).
- [23] S. Mangin, F. Montaigne, and A. Schuhl, Interface domain wall and exchange bias phenomena in ferrimagnetic/ferrimagnetic bilayers, *Phys. Rev. B* **68**, 140404(R) (2003).
- [24] J. Huang, C. Prados, J. E. Evetts, and A. Hernando, Giant magnetostriction of amorphous Tb_xFe_{1-x} ($0.10 < x < 0.45$) thin films and its correlation with perpendicular anisotropy, *Phys. Rev. B* **51**, 297 (1995).
- [25] P. Hansen, C. Clausen, G. Much, M. Rosenkranz, and K. Witter, Magnetic and magneto-optical properties of rare-earth transition metal alloys containing Gd, Tb, Fe, Co, *J. Appl. Phys.* **66**, 756 (1989).
- [26] B. Hebler, A. Hassdenteufel, P. Reinhardt, H. Karl, and M. Albrecht, Ferrimagnetic Tb-Fe alloy thin films: Composition and thickness dependence of magnetic properties and all-optical switching, *Front. Mater.* **3**, 8 (2016).
- [27] S. Mangin *et al.*, Engineered materials for all-optical helicity-dependent magnetic switching, *Nat. Mater.* **13**, 286 (2014).
- [28] M. H. Tang, Z. Zhang, S. Y. Tian, J. Wang, B. Ma, and Q. Y. Jin, Interfacial exchange coupling and magnetization reversal in perpendicular $[Co/Ni]_N/TbCo$ composite structures, *Sci. Rep.* **5**, 10863 (2015).
- [29] M. S. El Hadri, M. Hehn, P. Pirro, C.-H. Lambert, G. Malinowski, Eric E. Fullerton, and S. Mangin, Domain size criterion for the observation of all-optical helicity-dependent switching in magnetic thin films, *Phys. Rev. B* **94**, 064419 (2016).
- [30] G. Cliff and G. W. Lorimer, The quantitative analysis of thin specimens, *J. Microsc.* **103**, 203 (1975).
- [31] C. B. Hill, W. R. Hendren, R. M. Bowman, P. K. McGeekin, M. A. Gubbins, and V. A. Venugopal, Whole wafer magnetostriction metrology for magnetic films and multilayers, *Meas. Sci. Technol.* **24**, 045601 (2013).
- [32] K. K. Ho, K. P. Mohanchandra, and G. P. Carman, Examination of the sputtering profile of NiTi under target heating conditions, *Thin Solid Films* **413**, 1 (2002).
- [33] J. J. Rhyne, J. H. Schelleng, and N. C. Koon, Anomalous magnetization of amorphous $TbFe_2$, $GdFe_2$, and YFe_2 , *Phys. Rev. B* **10**, 4672 (1974).
- [34] R. Pellicelli, M. Solzi, C. Pernechele, and M. Ghidini, Continuum micromagnetic modeling of antiferromagnetically exchange-coupled multilayers, *Phys. Rev. B* **83**, 054434 (2011).
- [35] S. Jain, D. Tripathy, and A. O. Adeyeye, Investigating the exchange bias in multilayer triangular nanorings, *J. Appl. Phys.* **105**, 123916 (2009).
- [36] E. F. Kneller and R. Hawig, The exchange-spring magnet: A new material principle for permanent magnets, *IEEE Trans. Magn.* **27**, 3588 (1991).
- [37] Y. J. Nam and S. H. Lim, Negative remanent magnetization in a single domain particle with two uniaxial anisotropies, *Appl. Phys. Lett.* **99**, 092503 (2011).
- [38] C. Schubert, *Magnetic Order and Coupling Phenomena* (Springer, New York, 2014), Chap. 2, p. 5.
- [39] Shih-Cheng N. Cheng and Mark H. Kryder, Separation of perpendicular anisotropy components in dc-magnetron sputtered TbFe amorphous films, *J. Appl. Phys.* **69**, 7202 (1991).